Water-Soluble Mn(III)-Porphyrins with High Relaxivity and Photosensitization

Tamas Nemeth, Agnès Pallier, Çetin Çelik, Zoltán Garda, Naoko Yoshizawa-Sugata, Hisao Masai, Éva Tóth, Yoko Yamakoshi

ACS Partner Journal

CHEMICAL & BIOMEDICAL IMAGING

pubs.acs.org/ChemBioImaging

Article

Water-Soluble Mn(III)-Porphyrins with High Relaxivity and Photosensitization

Tamas Nemeth, Agnès Pallier, Çetin Çelik, Zoltán Garda, Naoko Yoshizawa-Sugata,* Hisao Masai,* Éva Tóth,* and Yoko Yamakoshi*

Cite This: https://doi.org/10.1021/cbmi.4c00046

Read Online

ACCESS | Metrics & More | Article Recommendations | Supporting Information

ABSTRACT: Three water-soluble Mn(III)-porphyrin complexes with cationic pyridyl side groups bearing COOH- or OH-terminated carbon chains in the meta or para positions have been synthesized as probes for both magnetic resonance imaging (MRI) and photodynamic therapy (PDT). The complexes **Mn-1**, **Mn-2**, and **Mn-3** are highly water-soluble, and their relaxivities range between 10 and 15 mM^{-1} s^{-1}, at 20−80 MHz and 298 K, 2−3 times higher than that of commercial Gd(III)-based agents. The complexes containing carboxylate (**Mn-2**) or alcoholic (**Mn-3**) side chains in the para position are endowed with higher relaxivities and have also shown efficient photoinduced DNA cleavage and singlet oxygen ($^1O_2$) generation. **Mn-3** with stronger photoinduced DNA cleavage has also revealed stabilizing and binding activities for G4 DNA, at a similar level as the known G4 binder **Mn-TMPyP4**. Nevertheless, the G4-binding activity of **Mn-3** was nonspecific. Preliminary tests evidenced photocytotoxicity of **Mn-3** on HeLa cells without a significant effect in the absence of light. Altogether, these results underline the potential of such water-soluble Mn(III)-porphyrins for the development of multimodal approaches combining MRI and PDT.

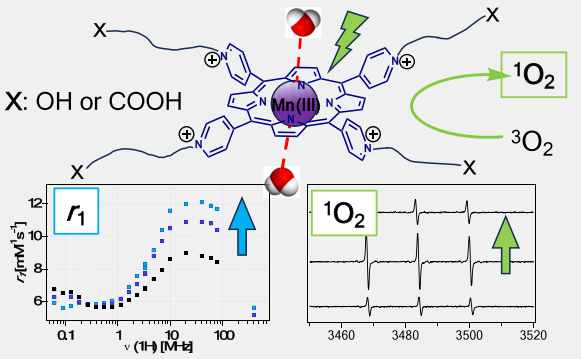

KEYWORDS: *MRI contrast agent, Mn(III)-porphyrin complex, relaxivity, ROS generation, photodynamic therapy*

INTRODUCTION

The design of efficient imaging probes, such as near-infrared (NIR) fluorophores, radioactive molecules, or paramagnetic metal complexes, has a pivotal role in the development of highly sensitive and functional in vivo imaging approaches based on optical, nuclear, or magnetic resonance imaging (MRI) modalities. Among these, MRI, which provides deep tissue images with excellent resolution, is regarded as a desirable, noninvasive technique that does not involve ionizing radiation hazards. To achieve a more effective contrast enhancement in MR images, paramagnetic contrast agents (MRI-CAs) are often injected into the body prior to the examination.

All MRI-CAs in current clinical use are Gd(III) complexes. Due to its seven unpaired electrons (S = 7/2) and slow electron spin relaxation, Gd(III) greatly enhances the relaxation process of water protons in the surrounding tissue.[1,2] However, Gd(III) is toxic in its free, noncomplexed form, and there has been increasing concern related to toxic side effects of Gd(III)-based MRI agents, especially in patients with chronic kidney diseases (CKD).[3−6] These include (i) rare, but serious pathologies, such as contrast-induced nephropathy (CIN)[7,8] and nephrogenic systemic fibrosis (NSF),[9] and (ii) the accumulation of Gd(III) in the brain of patients who received repeated Gd(III)-chelate injections.[10−15] To avoid these potential risks of Gd(III) complexes, Mn(II/III)-based contrast agents have recently attracted attention and are generally considered as sufficiently safe imaging probes.[16−19] Although Mn(III) contains only four unpaired electrons (S = 2), one less than Mn(II) (S = 5/2), some Mn(III) complexes such as porphyrins are endowed with elevated relaxivity at typical clinical magnetic fields (>1.5 T), where the efficacy of Mn(II) or Gd(III) chelates tend to decrease. In Mn(III)-porphyrin complexes, it is known that the metal is coordinated with an octahedral geometry involving planar coordination of the four equatorial pyrrolic nitrogens and two additional axial ligands.[11] In aqueous solutions, water molecules can occupy these axial positions. Mn(III)-porphyrins have long been investigated for their water proton relaxation efficacy, with a recent revival of this field.[20−31] Given the hydrophobic nature of porphyrins and their tendency to aggregate in aqueous solution, one of the key challenges in this field involves improvement of water-solubility. Lately, Mn-porphyrins have

Received: June 2, 2024
Revised: August 8, 2024
Accepted: August 12, 2024

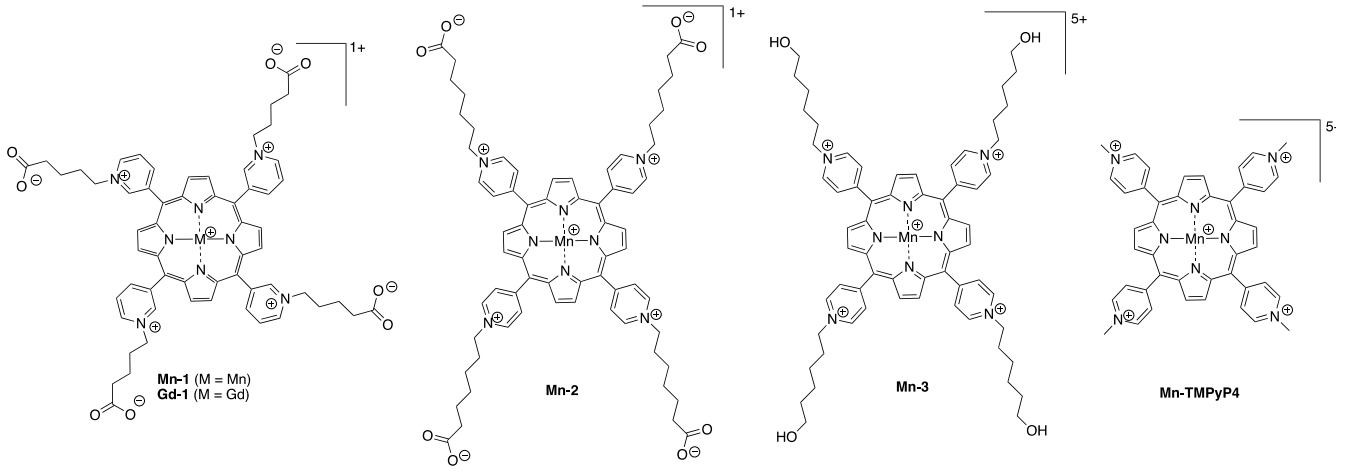

Figure 1. Structures of Gd(III)-porphyrin complex (**Gd-1**, previously reported[43]) and Mn(III)-porphyrin complexes (**Mn-1**, **Mn-2**, **Mn-3**, and **Mn-TMPyP4**).

been also explored as potential redox-sensitive MRI probes relying on the different relaxivity of the reduced Mn(II) and the oxidized Mn(III) forms.[30,32,33] In addition, some fluorinated derivatives have been studied as ^{19}F MRI probes.[34] Furthermore, porphyrins are also well-known in the field of photodynamic therapy (PDT) as efficient photosensitizers (PSs).[35] Many clinically approved PDT-PSs belong to the family of porphyrins.[36] The combination of photosensitizing and MRI contrast enhancement capabilities within a single molecular entity has been the subject of many studies, and again, porphyrin derivatives are among the most explored systems in this field.[37−42]

Recently, we have reported a Gd(III)-porphyrin complex (**Gd-1** in Figure 1) that offers high relaxivity as well as ROS generation and subsequent DNA cleavage under visible light irradiation.[43] While this complex was stable in a neutral buffer at physiological pH thanks to the supposed participation of the pending COO^- functions in Gd(III) coordination, undesired decomplexation was observed under lower pH (<5.5). This low stability is likely due to the large ionic radius of Gd(III), leading to a less stable out-of-plane coordination by the porphyrin nitrogens and to the weak binding of the distant carboxylates. Mn(III)-complexation by porphyrins, on the other hand, is known to be extremely stable, reducing the risk of free metal leakage. Therefore, we have investigated the Mn(III) complex of the same porphyrin chelator, **Mn-1**, as well as two additional water-soluble Mn(III)-porphyrins, **Mn-2** and **Mn-3** (Figure 1), with a cationic charge in the para positions. A specific objective of this study was to test the influence of the side chains attached to the porphyrin core, which bear either a negatively charged COO^- or a neutral OH terminal group. Field-dependent proton relaxivities, characterizing the efficacy of the complexes as potential MRI probes, were compared for these different systems. In addition, the photosensitivity[44] of porphyrins **2** and **3** and of their Mn(III)-complexes (**Mn-2** and **Mn-3**) has been studied by photo DNA cleavage, and $^1O_2$ generation as monitored by ESR in the presence of a spin-trapping agent. Further, their binding to oncogene-related guanine quadruplex (G4) DNA has been investigated by a FRET assay. Finally, photocytotoxicity tests were performed on HeLa cells. For comparison, in these studies, we have also included the known G4-binding molecule, **TMPyP4** and its Mn(III) complex as reference compounds (Figure 1).

EXPERIMENTAL SECTION

General

All reagents were purchased from Sigma-Aldrich Co. LLC (Merck KGaA, Darmstadt, Germany) unless described otherwise and purified as described when needed. Solvents were purchased from Acros Organic (Thermo Fischer Scientific, Inc., Geel, Belgium), and HPLC-grade solvents were purchased from Sigma-Aldrich Co. LLC (Merck KGaA), and dried by a solvent system (Innovative Technology Inc., Brooksville, FL) or distilled when needed. All water used was from Millipore purification system. Column chromatography and analytical TLC were performed, respectively, on SILICYCLE SilicaFlash F60 (230−400 mesh with pore size 60 Å) and silica gel 60 F254 TLC (Merck KGaA). Flash chromatographic purifications were performed on a Büchi Reveleris X2 flash purification system (Büchi Labortechnik AG, Flawil, Switzerland) using Büchi Reveleris C18 columns (PN 145171532) for reverse phase separation. NMR spectra were recorded at room temperature on a BrukerAV300 300 MHz spectrometer or a Bruker AV400 400 MHz spectrometer (Bruker BioSpin GmbH, Rheinstetten, Germany). The HR-MS data were obtained using a Bruker SolariX-FTICR 9.4 T MS instrument (Bruker Daltonics, Bremen, Germany). FT-IR spectra were recorded on a JASCO 4100 FT-IR spectrometer equipped with an ATR Pro One instrument (JASCO, Inc., Tokyo, Japan). The UV−vis spectra were measured on a Varian Cary-500 UV−vis spectrophotometer (Agilent, Santa Clara, CA) using a cuvette with 1 cm optical path (Quartz Cell, Type F15−UV-10, transmission 85.5%, GL Sciences Inc., Tokyo, Japan,).

Synthesis

Detailed procedures for the synthesis of new compounds (**3**, **Mn-1**−**3**) and the reference compound (**Mn-TmPyP4**) including their synthetic intermediates are described in SI with available spectroscopic data.

Relaxometric Measurements

^{1}H NMRD profiles of aqueous solutions of **Mn-1**, **Mn-2**, **Mn-3**, and **Mn-TMPyP4** in 0.1 M HEPES buffer (pH 7.4) were measured at 25 and 37 °C on a Stelar SMARtracer fast field cycling NMR relaxometer (0.00024−0.24 T, 0.01−10 MHz ^{1}H Larmor frequency) (Stelar s.r.l, Mede, Italy) and a Bruker WP80 NMR electromagnet adapted to variable-field measurements (0.47−1.88 T, 20−80 MHz), and controlled by the SMARtracer PC-NMR console. The temperature was controlled by a VTC91 control unit and maintained by a gas flow. The temperature was determined according to a previous calibration with a Pt resistance temperature probe. The relaxivity at 400 MHz was determined on a Bruker Advanced NMR spectrometer.

https://doi.org/10.1021/cbmi.4c00046
Chem. Biomed. Imaging XXXX, XXX, XXX−XXX

^{17}O NMR Studies

Variable-temperature ^{17}O chemical shifts and transverse relaxation rates were measured on aqueous solutions of **Mn-1** and **Mn-TMPyP4** on a Bruker Avance 400 MHz spectrometer using a 10 mm BBFO probe (9.4 T, 54.2 MHz) in the temperature range 5−75 °C. The temperature was calculated according to published calibration routines with ethylene glycol and MeOH.[45] Acidified water ($HClO_4$, pH 3.3) was used as a diamagnetic reference. Transverse ^{17}O relaxation times were obtained by the Carl−Purcell−Meiboom−Gill spin−echo technique. To eliminate susceptibility corrections to the chemical shifts, the sample was placed in a glass sphere fixed in a 10 mm NMR tube. To improve sensitivity, $H_2{}^{17}O$ (10% $H_2{}^{17}O$, CortecNet) was added to achieve ∼1% ^{17}O content in the sample. The pH of the samples was 7.0 (0.1 M HEPES buffer), and the complex concentrations were 2.45 mmol·kg^{-1} and 9.75 mmol·kg^{-1} for **Mn-1** and **Mn-TMPyP4**, respectively. The equations used for the analysis have been included in SI (section 2).

DNA Cleavage Tests

Photoirradiation was carried out using a green LED light source (λmax = 527 nm). A Mupid−exu gel electrophoresis apparatus (Takara Bio, Kyoto, Japan) was used for agarose gel electrophoresis. DNA cleavage studies were performed using supercoiled, covalently closed circular pBR 322 DNA (New England Biolabs, Ipswich, MA). Typically, a mixture of pBR 322 DNA (10 μL, 25 μg·mL^{-1} in Tris-HCl (10 mM)-EDTA (1 mM) buffer, pH = 8), 40 mM NADH (5 μL) or H_2O (5 μL) and 12.8 μM porphyrin aqueous solution (5 μL) was placed in a 0.5 mL Eppendorf tube. The tubes were placed with a distance of 2.5 cm from the green LED and exposed to the light for 0 or 4 h. Each resulting mixture (15 μL) was subjected to gel electrophoresis (1% agarose gel, in a 0.5x TBE buffer system at 100 V for 80 min). The gel was stained with ethidium bromide (1 μg·mL^{-1}) and was visualized on an ETX−35.M UV transilluminator (λ_{ex} = 312 nm, Vilber−Lourmat, Collégien, France) and photographed. The obtained images were analyzed using ImageJ software to quantify the amount of relaxed circular DNA (form II) relative to the intact DNA (form I).

$^1O_2$ Generation by the ESR Spin-Trapping Method

$^1O_2$ generation was measured by ESR using 2,2,6,6-tetramethyl-4-piperidone (4-oxo-TEMP, Acros, 98%) as a spin-trapping reagent. ESR spectra were recorded on a Bruker spectrometer (Bruker BioSpin GmbH) equipped with a microwave bridge X-band ER 082C. Light irradiation and ESR measurements were carried out on each sample in a disposable capillary with a 50 μL volume (cat. no. 120800, Blaubrand, Wertheim, Germany), which was placed inside an ESR tube with a 4 mm thin wall precision quartz, 250 mm in length (cat. no. Z567442, Wilmad, Vineland, NJ). As a standard sample, a known $^1O_2$-generating compound, Rose Bengal, was used. To an aliquot of porphyrin or Rose Bengal in D_2O (0.5 mM, 20 μL) were added 0.5 M 4-oxoTEMP (4 μL, in D_2O), 0.3 M phosphate buffer (10 μL, pH 7, in D_2O), and D_2O (16 μL) and mixed well under aerobic conditions. Each mixed solution was irradiated by green LED light (λ_{max} = 527 nm, PN 31867, Lumitronix, Hechingen, Germany) at a distance of 3 cm for 0, 1, 2, 5, and 10 min, introduced into a capillary, placed inside an ESR tube, and immediately subjected to the ESR measurements. The generation of $^1O_2$ was detected by the ESR signal corresponding to 4-oxo-TEMPO. Time-dependent data are shown in SI (section 5).

G4 Stabilization Assay by FRET

The G4 DNA (c-MYC, KIT or Rif1-2) labeled with FAM (5′ end) and TAMRA (3′ end) was denatured at 95 °C for 5 min at the concentration of 0.2 μM and subsequently incubated at room temperature to form the G4 structure. Each G4 DNA was mixed with each compound with concentrations of 0.25, 0.5, 1, 2, and 4 μM. The melting temperatures at each concentration were recorded on a LightCycler 480 II (Roche, Basel, Switzerland). FRET detection was carried out upon a temperature change from 37 to 95 °C with a ramp speed of 1 °C per minute.

G4 Binding Assay

Five picomole of the single-stranded oligonucleotide ^{32}P-labeled G4 DNA (parallel-type G4 T_6G_{24}) or non-G4 $T_6[GA]_{12}$ was heat-denatured and reannealed in the presence of 50 mM KCl and 40% PEG200. DNA was incubated with each porphyrin (0.1 and 1 nmol per reaction, or at the final concentration of 10 and 100 μM, respectively) at room temperature for 10 min in 40 mM HEPES-KOH (pH 7.6) containing 50 mM KCl, 1 mM EDTA, 10% glycerol, and 1 mM DTT. The complexes and free DNA were separated in 1% agarose gels in the presence of 0.1 M MES (pH 6.1) and 0.1 M histidine and detected by autoradiography on Hybond N+ filter (Cytiva, Tokyo, Japan). The detailed data are shown in SI (section 7).

Photocytotoxicity

A photocytotoxicity test was performed on HeLa cells and under irradiation from a green LED (527 nm) using an MTT assay. The details are described in SI (section 8).

Cytotoxicity

MCF-7, U2OS, or HeLa cells were precultured for 1 day in a 96-well plate (1 × 10^3 per well). The compounds were added at 2, 20, or 200 μM and incubated for an additional 2 days. Each culture medium was replaced with 1/10-diluted WST-1 reagent (Roche, Basel, Switzerland), the cells were treated for 2 h, and then the absorbances at 450 and 595 nm were monitored by iMark (Bio-Rad, Hercules, CA). The OD_{450} values were subtracted by OD_{595}. As a control experiment, samples without ligands were set as 100 and the relative values were calculated.

RESULTS AND DISCUSSION

Synthesis of Water-Soluble Mn(III)-Porphyrins Mn-1, Mn-2, and Mn-3

Water-soluble Mn(III)-porphyrin complex (**Mn-1**, Figure 1) was synthesized in a similar way to its analogous Gd(III)-chelate (**Gd-1**, Figure 1), which was recently reported.[43] Porphyrin **1** was prepared as previously reported and subjected to the complexation reaction using $MnCl_2$ followed by oxidation with air oxygen to provide a Mn(III)-complex (**Mn-1**) (Scheme S1). The obtained complex was purified by reversed phase HPLC and characterized by HR-ESI-MS (Figure S2), which confirmed the 1-to-1 stoichiometry of the Mn(III)-porphyrin complexation.

Figure 2 shows the UV−vis spectra of the free porphyrin ligand **1** and its Mn(III) complex **Mn-1** in comparison to the previously reported Gd(III) analogue **Gd-1**.[43] The Soret band of free ligand **1** has an absorption maximum at 418 nm, which shifted to 428 nm upon complexation with Gd(III) (**Gd-1**). It further red-shifted to 461 nm, with a smaller intensity, upon Mn(III) complexation (**Mn-1**), in full accordance with typical

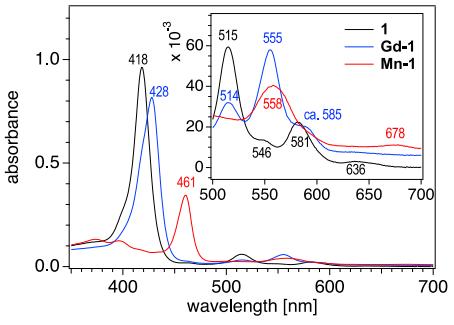

Figure 2. UV−vis spectra of porphyrin ligand **1** and its Mn(III)-complex (**Mn-1**) and Gd(III)-complex (**Gd-1**) at 12.5 μM in HEPES buffer (1 M, pH 7.4) at 25 °C.

https://doi.org/10.1021/cbmi.4c00046
Chem. Biomed. Imaging XXXX, XXX, XXX−XXX

absorption characteristics of Mn(III)-porphyrin complexes.[46] The position of this absorption band also confirms the oxidation of Mn(II) to the Mn(III) state.[34] Q-bands with four peaks in free **1** (maxima at 515, 546, 581, and 636 nm) changed upon metal complexation; the Gd(III)-complex (**Gd-1**) has three peaks (at 514, 555, and ca. 585 nm), indicating sitting atop (SAT) coordination structure, while the Mn(III)-complex (**Mn-1**) shows two bands (at 558 and 678 nm), suggesting higher symmetry in the structure. This can be explained by the planar metal coordination by the porphyrin in **Mn-1** that is related to the smaller ionic radius of Mn(III) in comparison to that of Gd(III), leading to a highly stable and inert chelate. In addition to the four pyrrole nitrogens coordinated in the porphyrin plane, two water molecules complete the coordination sphere in axial positions, above and below the porphyrin plane.

Two other Mn(III)-porphyrin complexes (**Mn-2** and **Mn-3**, Figure 1) with substitution at the para position of the pyridyl groups were synthesized. It was expected that COOH and OH groups, respectively, in the anchors of **Mn-2** and **Mn-3**, would help to increase water-solubility to provide the higher biocompatibility of the molecules. Porphyrin **2** was synthesized as previously reported.[43] Porphyrin **3** was synthesized by N-alykylation of pyridylporphyrin S1 with bromoalkyl alcohol (Schemes S3). As a control molecule, the Mn(III) complex of **TMPyP4** (**Mn-TMPyP4**) was prepared. These porphyrins, compounds **2**, **3**, and **TMPyP4**, formed complexes with Mn(III) in a 1-to-1 stoichiometry as confirmed by HR-ESI-MS (Figures S5, S13, and S19). All porphyrins and their corresponding Mn(III) complexes were thoroughly soluble in water. As shown in Figure 3a–c, changes in UV–vis absorption spectra of porphyrin upon Mn(III) complexation were observed in a similar manner as in the case of **Mn-1** (Figure 2), showing the red shift and decreased intensity of the Soret band and reduced peak numbers in Q-bands indicating the higher symmetry in the Mn(III) complex structure. These situations were in line with the previously reported Mn(III) complexes.[46]

A cyclic voltammetry study has been carried out on **Mn-1** (pH 6.9) and **Mn-TMPyP4** (pH 7.2) in 0.01 M HEPES buffer and yielded $E^\circ = -0.220$ V and -0.192 V (vs Ag/AgCl) for the midpoint potential of the Mn(II)/Mn(III) redox couple of the two complexes, respectively (see SI section 3 for details). The latter value is in good agreement with literature data.[47]

Relaxivity and ^{17}O NMR Studies of Mn(III)-Porphyrins

The efficacy of a paramagnetic complex to act as MRI-CAs is typically characterized by its relaxivity, which is the paramagnetic enhancement of the longitudinal water proton relaxation rate referred to as the 1 mM concentration of the probe. The capability of Mn(III)-porphyrin complexes to enhance MRI contrast has been evaluated by recording ^{1}H nuclear magnetic relaxation dispersion (NMRD) profiles at two different temperatures (25 and 37 °C), between 0.05 and 400 MHz, in HEPES buffer (0.1 M, pH 7.4). The ^{1}H NMRD profiles of **Mn-1**, **Mn-2**, **Mn-3**, and **Mn-TMPyP4** are depicted in Figure 4.

The shapes of these NMRD curves all presented a peak centered around 40–60 MHz, which was characteristic of Mn(III)-porphyrins, and the absolute relaxivity values fell also into the typical range reported for soluble, small-molecule Mn(III)-porphyrin complexes containing two inner sphere water molecules. Considerably decreased relaxivities have been

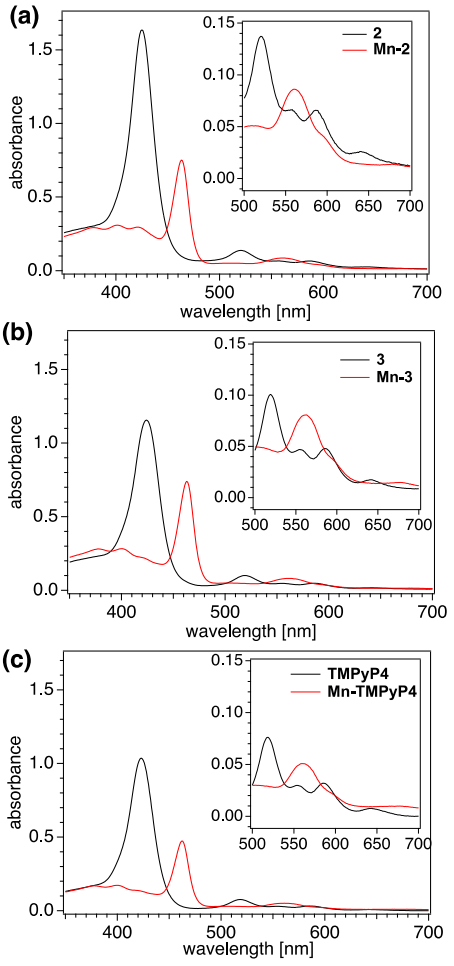

Figure 3. UV vis spectra of water-soluble cationic porphyrins **2** (a), **3** (b), and **TMPyP4** (c) and their Mn(III)-complexes **Mn-2**, **Mn-3**, and **Mn-TMPyP4** (12.5 μM in HEPES buffer (1 M, pH 7.4) at 25 °C).

reported for more hydrophobic Mn(III)-porphyrins which undergo extensive aggregation in aqueous solutions.[22,34] This clearly shows the importance of the charged groups appended on the porphyrin ring in ligands **1**, **2**, **3**, and **TMPyP4**, which maintain water-solubility. Indeed, aggregation was assumed to limit the exchange between the bound and solvent water molecules, which is very important for an efficient transfer of the paramagnetic relaxation effect of Mn(III) to the bulk.[22] We note that in contrast to **Gd-1**, the carboxylate functions do not coordinate to the central metal ion in **Mn-1**, leaving space for the coordination of two inner sphere water molecules. This difference is related to the larger size and higher coordination number of Gd(III), implying an out-of-plane position and the coordination by the carboxylate functions of this metal ion. On the other hand, Mn(III) fits perfectly into the porphyrin plane.

At all magnetic fields and at both temperatures, the relaxivities are very similar for **Mn-1** and **Mn-TMPyP4**. On the other hand, above ~5 MHz, **Mn-2** and **Mn-3** have considerably higher relaxivities. It is generally accepted that the analysis of the NMRD curves of Mn(III)-porphyrins is problematic in terms of the existing paramagnetic relaxation theory to extract the parameters characterizing the various microscopic and dynamic processes, such as water-exchange, rotational motion, or electron spin relaxation. These problems are largely related to the unusual role of zero field splitting

https://doi.org/10.1021/cbmi.4c00046
Chem. Biomed. Imaging XXXX, XXX, XXX–XXX

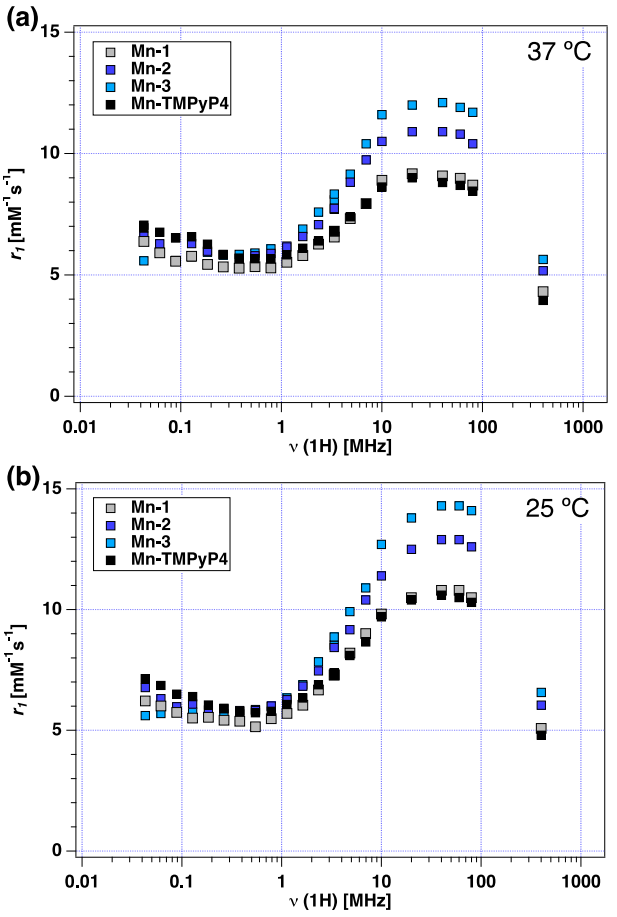

Figure 4. ^{1}H NMRD profiles of **Mn-1**−**3** and **Mn-TMPyP4** (1 mM in 0.1 M HEPES buffer (pH 7.4)) recorded at 37 °C (a) and 25 °C (b).

(ZFS) interactions and how these affect electron spin dynamics.[48,49] Nevertheless, we can draw several qualitative conclusions by comparing the relaxivity curves. The relatively similar low field relaxivities for all four systems suggest that their electron relaxation differences are not very important and cannot account for the different high-field values. Indeed, Bryant et al. have previously compared Mn(III)-porphyrin complexes endowed with different electron spin relaxation originating from the presence or the absence of bromine atoms at the β-pyrrole positions, leading to different delocalization of the electron spin density into the ligand.[21] They have demonstrated that electron spin relaxation affects both low- and high-field relaxivities. We can also exclude the effect of water exchange to account for the different proton relaxivities of **Mn-2** and **Mn-3** versus **Mn-1** and **Mn-TMPyP4**. The rate of water exchange has been previously assessed by ^{17}O NMR studies on various Mn(III) porphyrins bearing positive or negative charges and has been shown to be independent of the porphyrin charge. The measured rates ranged between 4 and 40 × 10^{6} s^{-1} (298 K).[50,51]

We have also assessed the water exchange rate by measuring variable temperature ^{17}O chemical shifts and transverse relaxation rates for aqueous solutions of **Mn-1** and **Mn-TMPyP4** at 9.4 T (Figure 5). The two complexes show very similar behavior, and the reduced chemical shifts and transverse relaxation rates are also similar to those reported for bishydrated Mn(III)-porphyrins in the literature.[50,51] This unambiguously shows the bishydrated nature of our complexes, indicating that the carboxylate functions in **Mn-1** are not coordinated to the metal ion. The ^{17}O NMR data have been analyzed according to the Swift−Connick equations (see SI for details).[52] The rate of the water exchange obtained from the fit is k_{ex}^{298} = (7.0 ± 0.4) × 10^{6} s^{-1} for both **Mn-1** and **Mn-TMPyP4**, while the activation enthalpy is 30 and 22 kJ·mol^{-1}, respectively, for the two complexes. Very similar exchange rates have been previously reported for analogous Mn(III)-porphyrins.[50,51]

These k_{ex} values imply that the water exchange is fast enough not to limit the relaxivity for such small molecular weight complexes. This is also evidenced by the increase of the relaxities with decreasing temperature. Therefore, the high-

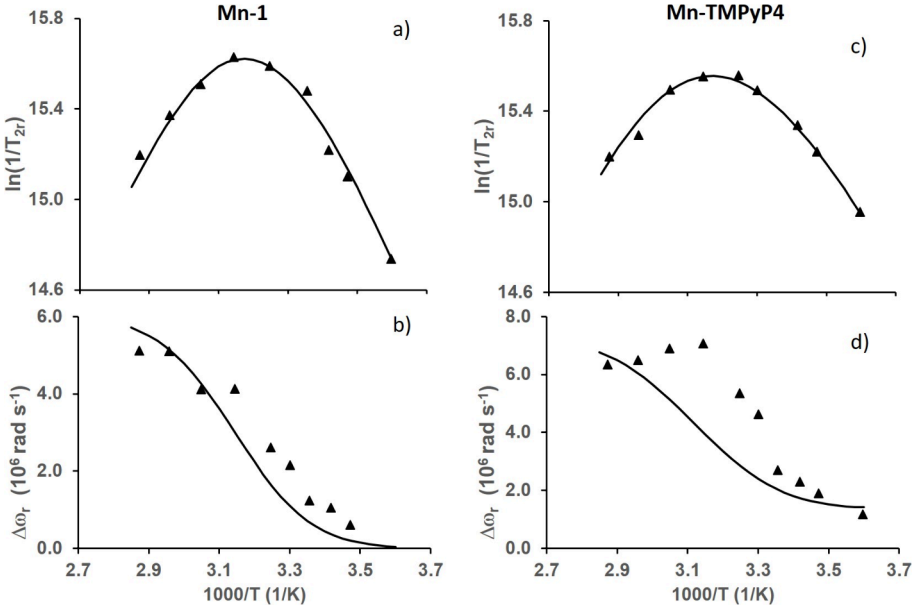

Figure 5. Variable temperature reduced ^{17}O transverse relaxation rates (a and c) and reduced chemical shifts (b and d) for **Mn-1** and **Mn-TMPyP4** complexes recorded at 9.4 T. The lines correspond to the fit of the data to the Swift−Connick equations (see SI section 2).

https://doi.org/10.1021/cbmi.4c00046
Chem. Biomed. Imaging XXXX, XXX, XXX−XXX

field differences in the relaxivities can be related to the different rotational motion of the chelates, as a consequence of their different size and molecular geometry. Globally, the higher relaxivities of **Mn-2** and **Mn-3** originate from their larger hydrodynamic size, related to the long (C6) pending chains introduced in the para position of the pyridine with respect to the porphyrin linkage. In **Mn-1**, the pendant chains are shorter and their orientation is different with respect to the porphyrin plane, which results in a more compact molecular structure for the complex. Interestingly, the relaxivities are practically identical at high fields for **Mn-1** and **Mn-TMPyP4**, despite their different molecular weight. One can speculate that a slightly slower electron spin relaxation of **Mn-TMPyP4** (indicated by the slightly higher relaxivities at low-field, where the effect of electronic relaxation is more important) compensates for its expectedly faster rotational motion, resulting in similar high-field relaxivities. The lower r_1 values observed for **Mn-2**, which bear charged carboxylic end-groups, versus **Mn-3** are somewhat surprising. This may be related to electrostatic attraction between the negatively charged carboxylate and the positively charged pyridine nitrogen, leading to a smaller hydrodynamic radius of the complex and thus faster rotational motion.

Beyond these differences, we can conclude that these Mn(III)-porphyrins, and in particular **Mn-2** and **Mn-3**, have very interesting relaxivities at clinically relevant magnetic fields, 2−3 times higher than that of commercially used MRI contrast agents (e.g., r_1 = 12.0 mM^{-1} s^{-1} for **Mn-3** versus r_1 = 3.8 mM^{-1} s^{-1} for GdDOTA, 20 MHz, 37 °C).[53] Their high water solubility is essential for this, since it prevents aggregation in aqueous solution, which would have negative consequences on the relaxivity.

Photoinduced DNA Cleavage

The Mn(III)-porphyrin chelates, **Mn-2** and **Mn-3**, were subjected to photo DNA cleavage tests to evaluate for their potential as PSs in PDT. A green LED with a dominant wavelength at 527 nm that overlaps with the absorption band of **Mn-2** and **Mn-3** was used. The amounts of generated nicked DNA (form II) were quantified by electrophoresis and subsequent staining with ethidium bromide. Significant DNA cleavage by **Mn-2** and **Mn-3** were observed under photoirradiation conditions (Figure 6). Especially, photoinduced DNA damage by **Mn-3** was evident, though a stronger activity

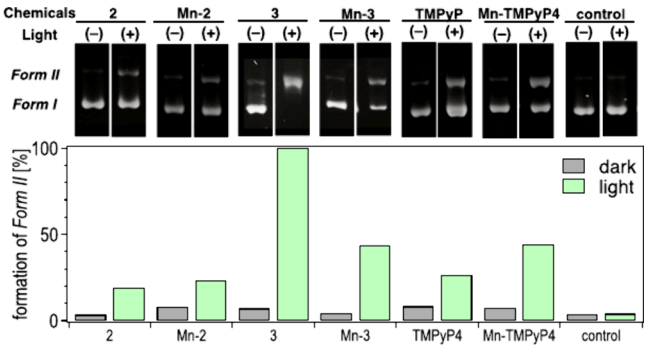

Figure 6. Photo DNA cleavage by **2**, **Mn-2**, **3**, **Mn-3**, **TMPyP4**, and **Mn-TMPyP4** under visible light irradiation. DNA: pBR322 supercoiled plasmid; photoirradiation: green LED (with dominant wavelength at 527 nm) for 4 h, 2.5 cm distance; porphyrins: 3.2 μM; in pH 8.0 Tris-HCl-EDTA buffer. Bottom: relative amount of form II generation under photoirradiation quantified by imageJ.

was observed with the free porphyrin **3**, presumably related to its higher absorption intensities at around 527 nm. Control experiments (1) under dark conditions with all compounds or (2) under light, but without any chemical, did not cause significant DNA cleavage, indicating that DNA cleavage occurred exclusively upon photoexcitation of the compounds.

Generation of $^1O_2$ under Visible Light Irradiation

$^1O_2$ is an important reactive oxygen species (ROS) involved in the photoinduced damages of biomolecules including DNA and often plays an essential role in PDT. The generation of $^1O_2$ by photoexcited **Mn-2** and **Mn-3** was evaluated by an ESR method using a spin-trapping reagent, 4-oxo-TEMP (see the scheme on the top of Figure 7).[54] As shown in Figures 7 and

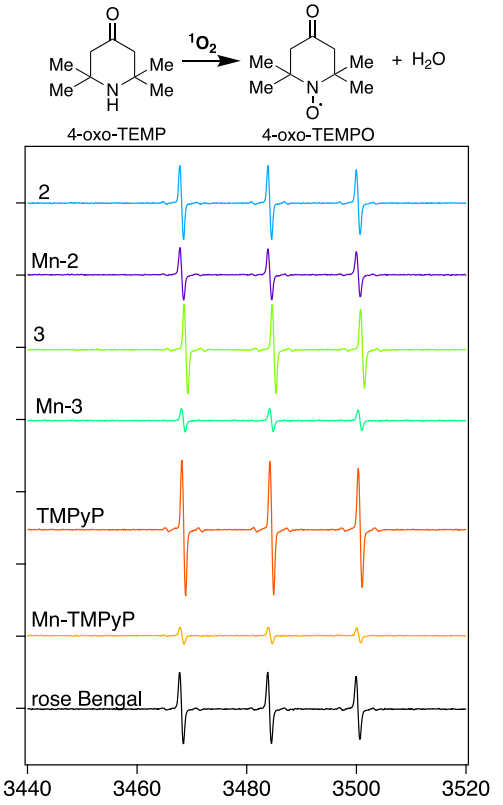

Figure 7. X-band ESR spectra for the $^1O_2$ adduct of 4-oxo-TEMP (4-oxo-TEMPO) generated by compounds **2**, **3**, and **TMPyP4** and their corresponding Mn(III)-complexes (**Mn-2**, **Mn-3**, and **Mn-TMPyP4**) solutions in D_2O (0.2 mM) in the presence of 50 mM 4-oxoTEMP. Photoirradiation: green LED (max 527 nm); distance: 3 cm; 10 min. Measurement conditions: temperature: 296 K; microwave frequency: 9.375 GHz; microwave power: 1 mW; modulation amplitude 4.00 G; modulation frequency: 100 kHz; scan time: 20.5 s. Rose Bengal was used as the standard PS for $^1O_2$ generation.

S29−35, the generation of 4-oxo-TEMPO ($^1O_2$ adduct of 4-oxo-TEMP) was observed in a time-dependent manner under irradiation from a green LED (527 nm at maximum). The $^1O_2$ generation was efficient in all Mn-porphyrin complexes (**Mn-2**, **Mn-3**, and **Mn-TMPyP4**) with slight differences, although the generation was decreased in comparison to their corresponding free porphyrins (Figure 7) in line with the data of photo DNA cleavages (Figure 6). This was presumably related to the absorption intensity of the compounds at the wavelength of the light used for photoirradiation, with a maximum at 527 nm. The paramagnetic Mn(III) ion can also have a quenching

https://doi.org/10.1021/cbmi.4c00046
Chem. Biomed. Imaging XXXX, XXX, XXX−XXX

effect on the $^1O_2$.[55] Taken together with the fact that **Mn-3** revealed high r_1 relaxivity (Figure 4) and sufficient photo DNA cleaving activity (Figure 5), this Mn(III)-porphyrin complex **Mn-3** can be regarded as a good candidate acting as a bifunctional molecular probe for both MRI-CA and PDT-PS.

Stabilization of G-Quadruplex (G4) DNA

TMPyP4 (Figure 1) has been known also as a G4-binding molecule due to its cationic moieties in the pyridyl side chains surrounding the rigid porphyrin skeleton.[56] G4-DNA-forming sequences are frequently present in the promoter regions of oncogenes, and a more prevalent existence of G4-DNA structures is one of the features of cancer cells, where the oncogenes are actively transcribed. We expected that the porphyrins **2** and **3** and their Mn(III)-complexes **Mn-2** and **Mn-3**, with structures having the same cationic patterns as **TMPyP4**, would have similar G4-binding activity and stabilize it, and that they may serve as novel G4-DNA sensing MRI agents to detect tumor tissues. Among them, porphyrin **3** with strong photo DNA cleavage (Figure 6) and $^1O_2$ generation (Figure 7) and its complex **Mn-3** with high relaxivity (Figure 4) were tested with respect to their G4 stabilizing ability.

G4 stabilization assays were conducted to monitor the G4-stabilizing effects on various G4-DNA structures. The FRET assays using three types of G4 DNAs (MYC, KIT, and Rif1-2) labeled with FAM and TAMRA at both 5′ and 3′ ends were performed on porphyrin **3**, **Mn-3**, **TMPyP4**, and **Mn-TMPyP4**. Compounds **3** and **Mn-3** revealed a dose-dependent increase of the melting temperature of all G4 DNAs tested (Figure 8a,b) indicative of G4-stabilizing effects, although the effects were weaker than with the control TMPyP4 (Figure 8c). Of note, the G4 stabilizing effect of **Mn-TMPyP4** was significantly attenuated (Figure 8d) compared to that of the metal-free **TMPyP4** (Figure 8c), whereas chelating Mn(III) to **3** did not cause a significant decrease in G4 stabilization (Figure 8b, in comparison with Figure 8a), indicating the possible dual properties of **Mn-3**, high relaxivity as a MRI agent and sustained G4-DNA stabilizing ability.

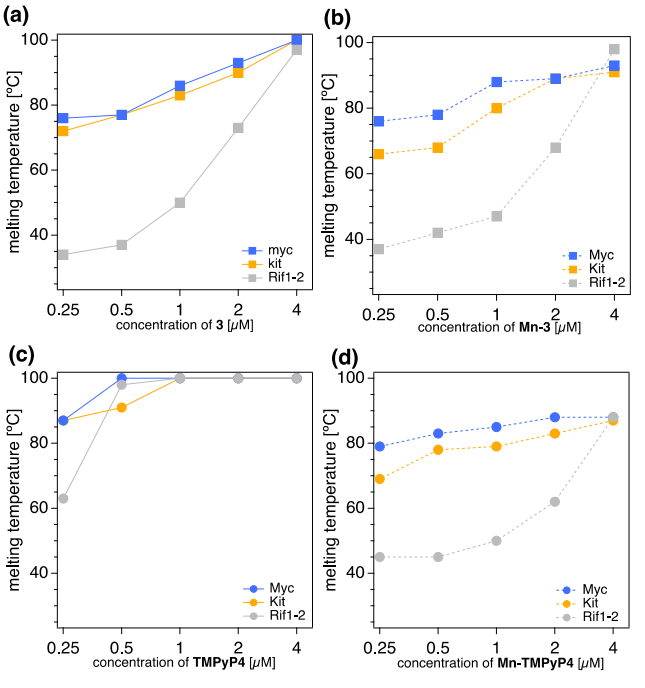

Figure 8. G4 stabilization assay of **3** (a), **Mn-3** (b), **TMPyP4** (c), and **Mn-TMPyP4** (d) by FRET. MYC, KIT, or Rif1-2 G4 DNA labeled with FAM and TAMRA at final 0.2 μM was formed by heat denaturation and annealing and mixed with each chemical at 0.25, 0.5, 1, 2, or 4 μM. FRET was detected during the temperature shift from 37 to 100 °C at the ramp speed of 1 °C·min^{-1}. The melting temperatures (T_m) at each concentration are shown. T_m values for c-MYC, c-KIT, and Rif1-2 DNA without binder are 75, 65, and 30 °C, respectively.

Binding to G4 DNA

G4-stabilizing agents interact with G4 DNA and regulate DNA transactions including DNA replication and transcription. The standard porphyrin **TMPyP4**, a known G4 DNA binder,[56] inhibits oncogene expression.[57] Based on the results above, G4 DNA-binding ability and selectivity were examined by an electrophoretic mobility shift assay (EMSA). To detect DNA–ligand complexes, G4 DNA (T6G24) or non-G4 DNA ($T6(GA)_{12}$) were coincubated with each compound, and the physical interaction was visualized after separation of the complexes and free DNA. As a result, **Mn-3** bound not only to G4 DNA but also to non-G4 DNA at 100 μM (Figure 9, lane 13). It should be noted that a control G4-binder **TMPyP4** did not clearly form complexes with G4 DNA (Figure 9, lanes 14 and 15) whereas **Mn-TMPyP4** weakly binds to G4 DNA at 100 μM, indicating that **Mn-3** has high DNA binding ability like **Mn-TMPyP4** but poor selectivity to G4 DNA structures under these experimental conditions. Similar results were observed in EMSA in acrylamide gels (Figure S37).

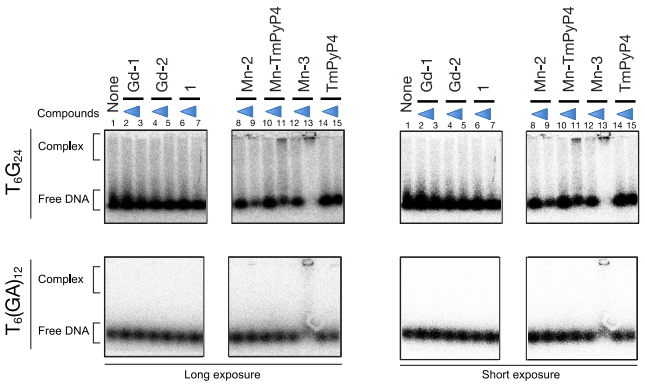

Figure 9. Binding of compounds to G4 DNA. One picomole of ^{32}P-labeled G4 DNA (parallel-type G4 T_6G_{24}) or non-G4 $T_6[GA]_{12}$ was incubated with the compounds (0.1 and 1 nmol; at the final concentration of 10 and 100 μM, respectively) in HEPES buffer containing 50 mM KCl at room temperature for 10 min. The products were separated on agarose gel and detected by autoradiography.

Photocytotoxicity

Following the results above, we tested the effect of **Mn-2**, **Mn-3**, and **Mn-TMPyP4** on the cells under visible light irradiation. A typical cancer cell line, cervical adenocarcinoma HeLa cells, have been used for these photocytotoxicity tests in combination with the MTT method.

As shown in Figure 10, significant photocytotoxicity was observed with all porphyrins (**2**, **3**, and **TMPyP4**) and their Mn-complexes (**Mn-2**, **Mn-3**, and **Mn-TMPyP4**). In line with photoinduced DNA cleavage, porphyrin **3** showed the highest photocytotoxicity, presumably related to the oxidative damage of biomolecules in the cells (e.g., cell membrane and other molecules). The highest photocytotoxicity of **Mn-3** among

https://doi.org/10.1021/cbmi.4c00046
Chem. Biomed. Imaging XXXX, XXX, XXX−XXX

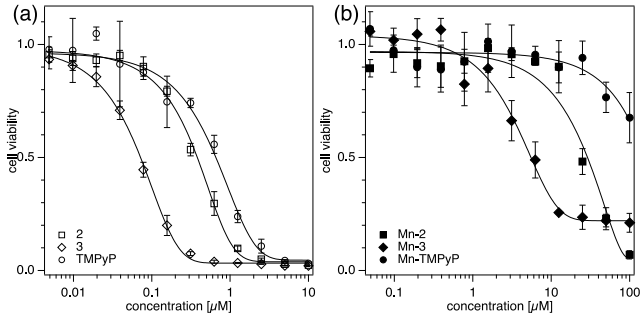

Figure 10. Photocytotoxicity of porphyrins (**2**, **3**, and **TMPyP4**) (a) and their Mn(III)-complexes (**Mn-2**, **Mn-3**, and **Mn-TMPyP4**) (b) on HeLa cells under green LED irradiation (527 nm, 45 mW per well). Irradiation was 15 min, and relative cell viability was measured by the MTT assay.

Mn(III)-complexes was observed (Figure 10b) although the efficiency in DNA cleavage (Figure 6) and $^1O_2$ generation (Figure 7) was similar to that of **Mn-TMPyP4**. This might be related to the other factors such as cell internalization efficiency. Further investigation is currently under process.

Cytotoxicity

Since the safety of imaging probes is the most important and critical issue when subjected to the living animals, cytotoxicity tests were performed as an initial assay on these porphyrins. For the quantification, the effect of **3**, **Mn-3**, **TMPyP4**, or **Mn-TMPyP4** on cell growth were tested with three cancer cell lines (Figure S39). All porphyrins showed low toxicity (IC_{50} > 100 μM) in osteosarcoma U2OS cells and HeLa cells, while the inhibitory effect of cell growth was observed in breast cancer MCF-7 cells. The IC_{50} values of **Mn-3** and **Mn-TMPyP4** were summarized in Table 1.

Table 1. Summary of Cytotoxicity and Photocytotoxicity of Mn-3 and Mn-TMPyP4

	IC_{50} [μM]			
	MCF-7	U2OS	HeLa	
complexes	dark	dark	dark	light
Mn-3	40.4	171	178	4
Mn-TMPyP4	13.2	167	>200	>100

Furthermore, the effects of Mn-porphyrins (**Mn-2**, **Mn-3**, and **Mn-TMPyP4**) and nonmetal chelated **3** on cell cycle profiles were analyzed (Figure S40). While the control experiments with L2H2-6OTD, a known G4 ligand, showed increases of sub-G1 population, which correlates with apoptotic cells with fragmentated DNA, experiments with other compounds did not cause significant changes.

CONCLUSION

Three water-soluble Mn(III)-porphyrin complexes, **Mn-1**−**3**, have been synthesized and investigated as potential MRI-CAs with photosensitizing capabilities. All three complexes are endowed with interesting r_1 relaxivities at clinically relevant magnetic fields, around 2−3 times higher than those of commercial Gd-based agents. The good water solubility of the Mn(III)-porphyrins is an important parameter for this, as it prevents porphyrin aggregation and subsequent relaxivity decrease often observed for more hydrophobic systems. **Mn-3**, with a tetracationic porphyrin structure similar to **TMPyP4** bearing charges on pyridine nitrogens in the para position, showed slight G4-DNA-stabilizing activity, although without selectivity over B-DNAs. Combined with the promising photosensitivity data (photoinduced DNA cleavage, $^1O_2$ generation, and photocytotoxicity), **Mn-3** can be considered as a potential core for the development of bimodal probes combining a good relaxation effect in MRI and therapeutic potential in PDT.

ASSOCIATED CONTENT

Supporting Information

The Supporting Information is available free of charge at https://pubs.acs.org/doi/10.1021/cbmi.4c00046.

Details of the syntheses of **Mn-1**, **2**, **Mn-2**, **3**, and **Mn-3** including their synthetic intermediates with necessary spectroscopic data, relaxivity measurements, photoinduced DNA cleavage, ROS generation measurements by ESR, FRET assay for G4 stabilization assay, G4-binding assay, and photocytotoxicity (PDF)

AUTHOR INFORMATION

Corresponding Authors

Naoko Yoshizawa-Sugata − *Research Center for Genome & Medical Sciences, Tokyo Metropolitan Institute of Medical Science, Setagaya, Tokyo 156-8506, Japan;* orcid.org/0000-0001-8792-8669; Email: yoshizawa-nk@igakuken.or.jp

Hisao Masai − *Department of Basic Medical Sciences, Tokyo Metropolitan Institute of Medical Science, Setagaya, Tokyo 156-8506, Japan;* orcid.org/0000-0003-1268-5302; Email: masai-hs@igakuken.or.jp

Éva Tóth − *Centre de Biophysique Moléculaire, CNRS UPR 4301, University of Orléans, 45071 Orléans, Cedex 2, France;* orcid.org/0000-0002-3200-6752; Email: eva.jakabtoth@cnrs.fr

Yoko Yamakoshi − *Department of Chemistry and Applied Biosciences, ETH Zürich, CH 8093 Zürich, Switzerland;* orcid.org/0000-0001-8466-0118; Email: yamakoshi@org.chem.ethz.ch

Authors

Tamas Nemeth − *Department of Chemistry and Applied Biosciences, ETH Zürich, CH 8093 Zürich, Switzerland;* orcid.org/0000-0003-4739-5882

Agnès Pallier − *Centre de Biophysique Moléculaire, CNRS UPR 4301, University of Orléans, 45071 Orléans, Cedex 2, France*

Çetin Çelik − *Department of Chemistry and Applied Biosciences, ETH Zürich, CH 8093 Zürich, Switzerland;* orcid.org/0000-0001-6132-8710

Zoltán Garda − *Centre de Biophysique Moléculaire, CNRS UPR 4301, University of Orléans, 45071 Orléans, Cedex 2, France;* orcid.org/0000-0002-3904-2959

Complete contact information is available at: https://pubs.acs.org/10.1021/cbmi.4c00046

Author Contributions

N.Y.-S., H.M., E.T., and Y.Y. designed the overall project. T.N. designed detailed structures of the molecules and contributed to their synthesis and structural characterization in collaboration with C.C. and Y.Y. A.P. performed relaxivity and ^{17}O

https://doi.org/10.1021/cbmi.4c00046
Chem. Biomed. Imaging XXXX, XXX, XXX−XXX

NMR measurements in collaboration with E.T. Z.G performed electrochemical measurements and analyses in collaboration with E.T. N.Y.-S. and H.M. performed G4 stabilization/binding activity assays and cytotoxicity tests. C.C. performed photocytotoxicity tests in collaboration with Y.Y. The manuscript was written with contributions of all authors. All authors have given approval to the final version of the manuscript.

Notes

The authors declare no competing financial interest.

■ ACKNOWLEDGMENTS

The authors thank Dr. Bertran Rubi from MoBiAS and Dr. Marc-Olivier Ebert from NMR service in the Department of Chemistry and Applied Biosciences at the ETH Zürich for their support on HR-MS and NMR measurements. The authors thank Ms. Naoko Kakusho and Ms. Hikari Miyamoto from Tokyo Metropolitan Institute of Medical Sciences for conducting G4-related assays. This research was supported in part by SNF Strategic Japanese-Swiss Science and Technology Program (IZLJZ2_183660, YY), JSPS, under the Joint Research Program implemented in association with SNF (20191508, H.M. and N.Y.-S), SNF Project Funding (205321_173018, Y.Y.), ETH Research Grants (ETH-21_15-2; ETH-36_20-2, Y.Y.), JSPS KAKENHI (Grant-in-Aid for Scientific Research [A], 6251004, H.M.; Grants-in-Aid for Scientific Research on Innovative Areas, 21H00264, 22H04707, H.M.; Grant-in-Aid for Scientific Research [C], 15K07164, N.Y.-S).

■ ABBREVIATIONS

MRI, magnetic resonance imaging; MRI-CA, magnetic resonance imaging contrast agent; PDT, photodynamic therapy; PS, photosensitizer; $^1O_2$, singlet oxygen; NIR, near-infrared; PET, positron emission tomography; CKD, chronic kidney disease; CIN, contrast induced nephropathy; NSF, nephrogenic systemic fibrosis; HPLC, high pressure liquid chromatography; TLC, thin layer chromatography; NMR, nuclear magnetic resonance; HRMS, high resolution mass spectrometry; FTIR, Fourier transfer infrared; ESR, electro spin resonance; 4-oxo-TEMP, 2,2,6,6-tetramethyl-4-piperidone; FRET, fluorescence resonance energy transfer; G4, guanine quadruplex; EMSA, electrophoretic mobility shift assay

■ REFERENCES

(1) Merbach, A.; Helm, L.; Tóth, É. *The Chemistry of Contrast Agents in Medical Magnetic Resonance Imaging*; John Wiley & Sons: Chichester, West Sussex, United Kingdom, 2013.

(2) Li, H.; Meade, T. J. Molecular Magnetic Resonance Imaging with Gd(III)-Based Contrast Agents: Challenges and Key Advances. *J. Am. Chem. Soc.* **2019**, *141* (43), 17025−17041.

(3) Toxicity of Gadolinium-Based Contrast Agents. *Med. Lett. Drugs. Ther.* **2007**, *49* (1262), 45.

(4) Bower, D. V.; Richter, J. K.; von Tengg-Kobligk, H.; Heverhagen, J. T.; Runge, V. M. Gadolinium-Based MRI Contrast Agents Induce Mitochondrial Toxicity and Cell Death in Human Neurons, and Toxicity Increases With Reduced Kinetic Stability of the Agent. *Invest. Radiol.* **2019**, *54* (8), 453−463.

(5) Khairinisa, M. A.; Amano, I.; Miyazaki, W.; Koibuchi, N.; Tsushima, Y. Gadolinium-Based Contrast Agents Toxicity in Animal Studies. *Magn. Reson. Imaging* **2019**, *62*, 57−58.

(6) Kong, Y.; Zhang, S.; Wang, J. L.; Han, C. P.; Yu, N. N.; Liu, Q.; Wang, W. T.; Xu, K. Potential Toxicity Evaluation and Comparison within Multiple Mice Organs after Repeat Injections of Linear *versus* Macrocyclic Gadolinium-Based Contrast Agents: A Comprehensive and Time Course Study. *Toxicol. Lett.* **2021**, *350*, 152−161.

(7) Nash, K.; Hafeez, A.; Hou, S. Hospital-Acquired Renal Insufficiency. *Am. J. Kidney Dis.* **2002**, *39* (5), 930−936.

(8) Solomon, R. J.; Natarajan, M. K.; Doucet, S.; Sharma, S. K.; Staniloae, C. S.; Katholi, R. E.; Labinaz, M.; Moreyra, A. E.; Gelormini, J. L. Cardiac angiography in Renally Impaired Patients (CARE) Study - A Randomized Double-Blind Trial of Contrast-Induced Nephropathy in Patients with Chronic Kidney Disease. *Circulation* **2007**, *115* (25), 3189−3196.

(9) Marckmann, P.; Skov, L.; Rossen, K.; Dupont, A.; Damholt, M. B.; Heaf, J. G.; Thomsen, H. S. Nephrogenic Systemic Fibrosis: Suspected Causative Role of Gadodiamide Used for Contrast-Enhanced Magnetic Resonance Imaging. *J. Am. Soc. Nephrol.* **2006**, *17* (9), 2359−2362.

(10) Kanda, T.; Fukusato, T.; Matsuda, M.; Toyoda, K.; Oba, H.; Kotoku, J.; Haruyama, T.; Kitajima, K.; Furui, S. Gadolinium-Based Contrast Agent Accumulates in the Brain Even in Subjects without Severe Renal Dysfunction: Evaluation of Autopsy Brain Specimens with Inductively Coupled Plasma Mass Spectroscopy. *Radiology* **2015**, *276* (1), 228−232.

(11) Kanda, T.; Osawa, M.; Oba, H.; Toyoda, K.; Kotoku, J.; Haruyama, T.; Takeshita, K.; Furui, S. High Signal Intensity in Dentate Nucleus on Unenhanced T_1-weighted MR Images: Association with Linear *versus* Macrocyclic Gadolinium Chelate Administration. *Radiology* **2015**, *275* (3), 803−809.

(12) Kanda, T.; Ishii, K.; Kawaguchi, H.; Kitajima, K.; Takenaka, D. High Signal Intensity in the Dentate Nucleus and Globus Pallidus on Unenhanced T_1-weighted MR Images: Relationship with Increasing Cumulative Dose of a Gadolinium-Based Contrast Material. *Radiology* **2014**, *270* (3), 834−841.

(13) McDonald, R. J.; McDonald, J. S.; Kallmes, D. F.; Jentoft, M. E.; Paolini, M. A.; Murray, D. L.; Williamson, E. E.; Eckel, L. J. Gadolinium Deposition in Human Brain Tissues after Contrast-Enhanced MR Imaging in Adult Patients without Intracranial Abnormalities. *Radiology* **2017**, *285* (2), 546−554.

(14) McDonald, R. J.; McDonald, J. S.; Kallmes, D. F.; Jentoft, M. E.; Murray, D. L.; Thielen, K. R.; Williamson, E. E.; Eckel, L. J. Intracranial Gadolinium Deposition after Contrast-Enhanced MR Imaging. *Radiology* **2015**, *275* (3), 772−782.

(15) Kanal, E.; Tweedle, M. F. Residual or Retained Gadolinium: Practical Implications for Radiologists and Our Patients. *Radiology* **2015**, *275* (3), 630−634.

(16) Gale, E. M.; Atanasova, I. P.; Blasi, F.; Ay, I.; Caravan, P. A Manganese Alternative to Gadolinium for MRI Contrast. *J. Am. Chem. Soc.* **2015**, *137* (49), 15548−15557.

(17) Geraldes, C. F. G. C.; Castro, M. M. C. A.; Peters, J. A. Mn(III) Porphyrins as Potential MRI Contrast Agents for Diagnosis and MRI-Guided Therapy. *Coordin. Chem. Rev.* **2021**, *445*, 214069.

(18) Pan, D.; Schmieder, A. H.; Wickline, S. A.; Lanza, G. M. Manganese-Based MRI Contrast Agents: Past, Present and Future. *Tetrahedron* **2011**, *67* (44), 8431−8444.

(19) Gale, E. M.; Jones, C. M.; Ramsay, I.; Farrar, C. T.; Caravan, P. A Janus Chelator Enables Biochemically Responsive MRI Contrast with Exceptional Dynamic Range. *J. Am. Chem. Soc.* **2016**, *138* (49), 15861−15864.

(20) Koenig, S. H.; Brown, R. D., 3rd; Spiller, M. The Anomalous Relaxivity of Mn^{3+} (TPPS4). *Magn. Reson. Med.* **1987**, *4* (3), 252−260.

(21) Bryant, L. H.; Hodges, M. W.; Bryant, R. G. Test of Electron Delocalization Effects on Water-Proton Spin-Lattice Relaxation by Bromination of [Tetrakis(4-sulfonatopheny)porphine]manganese. *Inorg. Chem.* **1999**, *38* (5), 1002−1005.

(22) Kellar, K. E.; Foster, N. Relaxation Enhancement of Water Protons by Manganese(III) Porphyrins - Influence of Porphyrin Aggregation. *Inorg. Chem.* **1992**, *31* (8), 1353−1359.

(23) Jing, L.; Liang, X.; Li, X.; Yang, Y.; Dai, Z. Covalent attachment of Mn-porphyrin onto doxorubicin-loaded poly(lactic acid) nano-

https://doi.org/10.1021/cbmi.4c00046
Chem. Biomed. Imaging XXXX, XXX, XXX−XXX

particles for potential magnetic resonance imaging and pH-sensitive drug delivery. *Acta Biomater* **2013**, *9* (12), 9434−41.
(24) Zou, T.; Zhen, M.; Chen, D.; Li, R.; Guan, M.; Shu, C.; Han, H.; Wang, C. The Positive Influence of Fullerene Derivatives Bonded to Manganese(III) Porphyrins on Water Proton Relaxation. *Dalton Trans.* **2015**, *44* (19), 9114−9119.
(25) Cheng, W.; Haedicke, I. E.; Nofiele, J.; Martinez, F.; Beera, K.; Scholl, T. J.; Cheng, H. L.; Zhang, X. A. Complementary Strategies for Developing Gd-Free High-Field T_1 MRI Contrast Agents Based on Mn(III) Porphyrins. *J. Med. Chem.* **2014**, *57* (2), 516−520.
(26) MacDonald, T. D.; Liu, T. W.; Zheng, G. An MRI-Sensitive, Non-Photobleachable Porphysome Photothermal Agent. *Angew. Chem., Int. Ed. Engl.* **2014**, *53* (27), 6956−6959.
(27) Westmeyer, G. G.; Emer, Y.; Lintelmann, J.; Jasanoff, A. MRI-Based Detection of Alkaline Phosphatase Gene Reporter Activity Using a Porphyrin Solubility Switch. *Chem. Biol.* **2014**, *21* (3), 422−429.
(28) Haedicke, I. E.; Li, T.; Zhu, Y. L. K.; Martinez, F.; Hamilton, A. M.; Murrell, D. H.; Nofiele, J. T.; Cheng, H. M.; Scholl, T. J.; Foster, P. J.; Zhang, X. A. An Enzyme-Activatable and Cell-Permeable Mn(III)-Porphyrin as a Highly Efficient T_1 MRI Contrast Agent for Cell Labeling. *Chem. Sci.* **2016**, *7* (7), 4308−4317.
(29) Lee, T.; Zhang, X. A.; Dhar, S.; Faas, H.; Lippard, S. J.; Jasanoff, A. *In Vivo* Imaging with a Cell-Permeable Porphyrin-Based MRI Contrast Agent. *Chem. Biol.* **2010**, *17* (6), 665−673.
(30) Calvete, M. J. F.; Pinto, S. M. A.; Pereira, M. M.; Geraldes, C. F. G. C. Metal Coordinated Pyrrole-Based Macrocycles as Contrast Agents for Magnetic Resonance Imaging Technologies: Synthesis and Applications. *Coordin. Chem. Rev.* **2017**, *333*, 82−107.
(31) Zhang, X. A.; Lovejoy, K. S.; Jasanoff, A.; Lippard, S. J. Water-Soluble Porphyrins as a Dual-Function Molecular Imaging Platform for MRI and Fluorescence Zinc Sensing. *Proc. Natl. Acad. Sci. U.S.A.* **2007**, *104* (26), 10780−10785.
(32) Pinto, S. M.; Tomé, V.; Calvete, M. J. F.; Castro, M. M. C. A.; Tóth, E.; Geraldes, C. F. G. C. Metal-Based Redox-Responsive MRI Contrast Agents. *Coordin. Chem. Rev.* **2019**, *390*, 1−31.
(33) Aime, S.; Botta, M.; Gianolio, E.; Terreno, E. A $p(O_2)$-Responsive MRI Contrast Agent Based on the Redox Switch of Manganese(II/III) - Porphyrin Complexes. *Angew. Chem., Int. Ed.* **2000**, *39* (4), 747−750.
(34) Pinto, S. M. A.; Ferreira, A. R. R.; Teixeira, D. S. S.; Nunes, S. C. C.; Batista de Carvalho, A. L. M.; Almeida, J. M. S.; Garda, Z.; Pallier, A.; Pais, A. A. C. C.; Brett, C. M. A.; Tóth, E.; Marques, M. P. M.; Pereira, M. M.; Geraldes, C. F. G. C. Fluorinated Mn(III)/(II)-Porphyrin with Redox-Responsive ^{1}H and ^{19}F Relaxation Properties. *Chem.-Eur. J.* **2023**, *29*, No. e202301442.
(35) Dougherty, T. J.; Gomer, C. J.; Henderson, B. W.; Jori, G.; Kessel, D.; Korbelik, M.; Moan, J.; Peng, Q. Photodynamic Therapy. *J. Natl. Cancer. Inst.* **1998**, *90* (12), 889−905.
(36) Lan, M. H.; Zhao, S. J.; Liu, W. M.; Lee, C. S.; Zhang, W. J.; Wang, P. F. Photosensitizers for Photodynamic Therapy. *Adv. Healthc. Mater.* **2019**, *8*, No. 1900132.
(37) He, M. E.; Chen, Y. A.; Tao, C.; Tian, Q. Q.; An, L.; Lin, J. M.; Tian, Q. W.; Yang, H.; Yang, S. P. Mn-Porphyrin-Based Metal-Organic Framework with High Longitudinal Relaxivity for Magnetic Resonance Imaging Guidance and Oxygen Self-Supplementing Photodynamic Therapy. *ACS Appl. Mater. Interfaces* **2019**, *11* (45), 41946−41956.
(38) Chen, Y. X.; Ma, Y. X.; Shi, K. X.; Chen, H.; Han, X.; Wei, C. X.; Lyu, Y.; Huang, Y. K.; Yu, R. H.; Song, Y.; Song, Q. X.; Jiang, J. Y.; Feng, J. F.; Lin, Y. Y.; Chen, J.; Chen, H. Z.; Zheng, G.; Gao, X. L.; Jiang, G. Self-Disassembling and Oxygen-Generating Porphyrin-Lipoprotein Nanoparticle for Targeted Glioblastoma Resection and Enhanced Photodynamic Therapy. *Adv. Mater.* **2024**, *36*, No. 2307454.
(39) Guidolin, K.; Ding, L. L.; Chen, J.; Wilson, B. C.; Zheng, G. Porphyrin-Lipid Nanovesicles (Porphysomes) are Effective Photosensitizers for Photodynamic Therapy. *Nanophotonics* **2021**, *10* (12), 3161−3168.
(40) Sour, A.; Jenni, S.; Ortí-Suárez, A.; Schmitt, J.; Heitz, V.; Bolze, F.; Loureiro de Sousa, P.; Po, C.; Bonnet, C. S.; Pallier, A.; Tóth, É.; Ventura, B. Four Gadolinium(III) Complexes Appended to a Porphyrin: A Water-Soluble Molecular Theranostic Agent with Remarkable Relaxivity Suited for MRI Tracking of the Photosensitizer. *Inorg. Chem.* **2016**, *55* (9), 4545−4554.
(41) Schmitt, J.; Jenni, S.; Sour, A.; Heitz, V.; Bolze, F.; Pallier, A.; Bonnet, C. S.; Tóth, E.; Ventura, B. A Porphyrin Dimer-GdDOTA Conjugate as a Theranostic Agent for One- and Two-Photon Photodynamic Therapy and MRI. *Bioconjugate Chem.* **2018**, *29* (11), 3726−3738.
(42) Jenni, S.; Bolze, F.; Bonnet, C. S.; Pallier, A.; Sour, A.; Tóth, É.; Ventura, B.; Heitz, V. Synthesis and *In Vitro* Studies of a Gd(DOTA)-Porphyrin Conjugate for Combined MRI and Photodynamic Treatment. *Inorg. Chem.* **2020**, *59* (19), 14389−14398.
(43) Nemeth, T.; Yoshizawa-Sugata, N.; Pallier, A.; Tajima, Y.; Ma, Y.; Toth, E.; Masai, H.; Yamakoshi, Y. Water-Soluble Gd(III)-Porphyrin Complexes Capable of Both Photosensitization and Relaxation Enhancement. *Chem. Biomed. Imaging* **2023**, *1* (2), 157−167.
(44) Xue, X. D.; Lindstrom, A.; Li, Y. P. Porphyrin-Based Nanomedicines for Cancer Treatment. *Bioconjugate Chem.* **2019**, *30* (6), 1585−1603.
(45) Raiford, D. S.; Fisk, C. L.; Becker, E. D. Calibration of Methanol and Ethylene-Glycol Nuclear Magnetic-Resonance Thermometers. *Anal. Chem.* **1979**, *51* (12), 2050−2051.
(46) Boucher, L. J. Manganese Porphyrin Complexes III. Spectroscopy of Chloroaquo Complexes of Several Porphhrins. *J. Am. Chem. Soc.* **1970**, *92* (9), 2725−2730.
(47) Ruhlmann, L.; Nakamura, A.; Vos, J. G.; Fuhrhop, J. H. Manganese Porphyrin Heterodimers and -Trimers in Aqueous Solution. *Inorg. Chem.* **1998**, *37* (23), 6052−6059.
(48) Schaefle, N.; Sharp, R. NMR Paramagnetic Relaxation of the Spin 2 Complex Mn^{III}TSPP: A Unique Mechanism. *J. Phys. Chem. A* **2005**, *109* (15), 3267−3275.
(49) Sharp, R.; Lohr, L.; Miller, J. Paramagnetic NMR Relaxation Enhancement: Recent Advances in Theory. *Prog. Nucl. Mag. Res. Sp.* **2001**, *38* (2), 115−158.
(50) Lieb, D.; Zahl, A.; Shubina, T. E.; Ivanovic-Burmazovic, I. Water Exchange on Manganese(III) Porphyrins. Mechanistic Insights Relevant for Oxygen Evolving Complex and Superoxide Dismutation Catalysis. *J. Am. Chem. Soc.* **2010**, *132* (21), 7282−7284.
(51) Budimir, A.; Kalmár, J.; Fábián, I.; Lente, G.; Bányai, I.; Batinic-Haberle, I.; Birus, M. Water Exchange Rates of Water-Soluble Manganese(III) Porphyrins of Therapeutical Potential. *Dalton Trans.* **2010**, *39* (18), 4405−4410.
(52) Swift, T. J.; Connick, R. E. NMR-Relaxation Mechanisms of O^{17} in Aqueous Solutions of Paramagnetic Cations and the Lifetime of Water Molecules in the First Coordination Sphere. *J. Chem. Phys.* **1962**, *37* (2), 307−320.
(53) Livramento, J. B.; Helm, L.; Sour, A.; O'Neil, C.; Merbach, A. E.; Tóth, E. A Benzene-Core Trinuclear Gd^{III} complex: Towards the Optimization of Relaxivity for MRI Contrast Agent Applications at High Magnetic Field. *Dalton Trans.* **2008**, 1195−1202.
(54) Lion, Y.; Delmelle, M.; Vandevorst, A. New Method of Detecting Singlet Oxygen Production. *Nature* **1976**, *263* (5576), 442−443.
(55) Porter, G.; Wright, M. R. Modes of Energy Transfer from Excited and Unstable Ionized States. Intramolecular and Intermolecular Energy Conversion Involving Change of Multiplicity. *Discuss. Faraday Soc.* **1959**, *27*, 18−27.
(56) Anantha, N. V.; Azam, M.; Sheardy, R. D. Porphyrin Binding to Quadruplexed T_4G_4. *Biochemistry* **1998**, *37* (9), 2709−2714.
(57) Siddiqui-Jain, A.; Grand, C. L.; Bearss, D. J.; Hurley, L. H. Direct Evidence for a G-Quadruplex in a Promoter Region and Its Targeting with a Small Molecule to Repress c-*MYC* Transcription. *Proc. Natl. Acad. Sci. U.S.A.* **2002**, *99* (18), 11593−11598.

https://doi.org/10.1021/cbmi.4c00046
Chem. Biomed. Imaging XXXX, XXX, XXX−XXX